Development on risk assessment model of urban ventilation based on COVID-19 pollution: a case study of an innovation base in Chongqing

Development on risk assessment model of urban ventilation based on COVID-19 pollution——A case study of an Innovation Base in Chongqing

Journal of Building and Environment

https://doi.org/10.1016/j.buildenv.2024.111431

Yongqiang Li[1, 2, *], Huangwei Zhang[2, 3], Runming Yao[4, 5], Ziqiao Li[4]

1. Faculty of Architecture and Urban Planning, Chongqing University, Chongqing, China.

2. National University of Singapore (Chongqing) Research Institute, Chongqing, China.

3. Department of Mechanical Engineering, National University of Singapore (NUS), Singapore.

4. School of Civil Engineering, Chongqing University, China.

5. School of Building Engineering, Reading University, UK.

* yongqiang.li@nusricq.cn

Abstract

Numbers of constructions have emerged due to the continuous urbanization process and the diversity of building clusters. Meanwhile, frequent global epidemics, such as COVID-19, have raised higher requirements for efficient urban ventilation. Traditional building design is insufficient to quantitatively consider the rationality of urban ventilation and corresponding risk assessments. This study carries out urban safety ventilation research and provides risk assessment models by using simulation and mathematical induction based on on-site measurement data, to realize accurate evaluation of disturbance of building clusters in urban environment, taking an Innovation Base in Chongqing as an example. The Amplification Coefficients on Urban Disturbance (ACUD) of the Innovation Base are respectively σ_1=0.047 representing safe evacuation distance for ventilation of new buildings downstream, σ_2=0.403 representing origin airflow disturbance retreat of new

buildings, σ_3=1.261 representing the control range of skyline design, and σ_4=4.381 representing urban canopy ventilation boundary. The Comprehensive Risk Coefficient (CRC) of the Innovation Base in the horizontal & vertical direction of CRC_h=17.88 and CRC_v=102.97 is obtained indicating the infection risk of residents in the vertical direction is 5.76 times greater than that in the horizontal direction. The Comprehensive Pollution Disturbance (CPD) is $1.70692*10^{-19}$ kg/m^3 which can be regarded as the quantitative risk assessment index of the Innovation Base under large public health safety events. This study contributes to effective support of architectural and urban design facing safe ventilation, providing theoretical support for the risk assessments, the resident control and anti-epidemic policies for both governments and residents during the worldwide epidemic situation.

Keywords

Urban ventilation; Air pollution; Risk assessment; Architectural design

List of symbols

Nomenclature	
A	Area (m^2)
AD	Average Deviation
Am*n	m * n-order matrix
A^Tm*n	Rank conversion of matrix of order m * n
CPD	Comprehensive Pollution Disturbance (dimensionless)
CPD_h	Comprehensive Pollution Disturbance in horizontal direction (dimensionless)
CPDv	Comprehensive Pollution Disturbance in vertical direction (dimensionless)
CRC	Comprehensive Risk Coefficient (dimensionless)
CRC_h	Comprehensive Risk Coefficient in Horizontal Direction (dimensionless)
CRC_v	Comprehensive Risk Coefficient in Vertical Direction (dimensionless)
CV	Coefficient of Variation (dimensionless)
D	Density (kg/m^3)
D_i	Density of ΔS_i (kg/m^3)
D_{hi}	Density of ΔS_i in horizontal direction (kg/m^3)
D_{vi}	

	Density of ΔS_i in vertical direction (kg/m^3)
ED	Eddy Viscosity (Pa*s)
ED_G	Eddy Viscosity Gradient (kg/m^2s)
ED_{Gx}	Eddy Viscosity Gradient in X dimension (kg/m^2s)
ED_{Gy}	Eddy Viscosity Gradient in Y dimension (kg/m^2s)
ED_{Gz}	Eddy Viscosity Gradient in Z dimension (kg/m^2s)
KU	Kurtosis (dimensionless)
M_i	Star masses of Planet i (kg)
n	Size of the sample
Nor	Normalization process
P_{ci}	Percentage of area of ΔS_i (m^2)
P_{chi}	Percentage of area of ΔS_i in horizontal direction (m^2)
P_{cvi}	Percentage of area of ΔS_i in vertical direction (m^2)
P_e	Foreign Planet into Pg
P_g	Ideal Plane Galaxy
P_i	Planet i within the ideal plane galaxy
PMC	Particle Mass Concentration (kg/m^3)
PMC_G	Particle Mass Concentration Gradient (kg/m^4)
PMC_{Gx}	Particle Mass Concentration Gradient in X dimension (kg/m^4)
PMC_{Gy}	Particle Mass Concentration Gradient in Y dimension (kg/m^4)
PMC_{Gz}	Particle Mass Concentration Gradient in Z dimension (kg/m^4)
r_i	Distance between Planet i and Planet e (m)
SD	Standard Division (dimensionless)
S_i	Occupying Areas of Planet i (m^2)
SKEW	Skewness (dimensionless)
TED	Turbulence Eddy Dissipation(m^2/s^3)
TED_G	Turbulence Eddy Dissipation Gradient
TED_{Gx}	Turbulence Eddy Dissipation in X dimension (m/s^3)
TED_{Gy}	Turbulence Eddy Dissipation in Y dimension(m/s^3)
TED_{Gz}	Turbulence Eddy Dissipation in Z dimension(m/s^3)
TKE	Turbulence Kinetic Energy (m^2/s^2)
TKE_G	Turbulence Kinetic Energy Gradient(m/s^2)
TKE_{Gx}	Turbulence Kinetic Energy Gradient in X dimension(m/s^2)
TKE_{Gy}	Turbulence Kinetic Energy Gradient in Y dimension(m/s^2)
TKE_{Gz}	Turbulence Kinetic Energy Gradient in Z dimension(m/s^2)
V	Velocity (m/s)
V_u	Velocity in X dimension (1/s)
V_v	Velocity in Y dimension (1/s)

$\mathbf{V_w}$	Velocity in Z dimension (1/s)
WS	Wall Share (Pa)
$\mathbf{WS_x}$	Wall Share in X dimension (Pa/m)
$\mathbf{WS_y}$	Wall Share in Y dimension (Pa/m)
$\mathbf{WS_z}$	Wall Share in Z dimension (Pa/m)
$\Delta \mathbf{S_i}$	Equally divided stars with the same size (kg/m_3)
ρ_i	Density of Planet i (kg/m^3)

1 Introduction

The world urbanization rate has risen to 48% at the end of the 20th Century and will eventually exceed 80% in the next 30 years[1]. Meanwhile, the coronavirus epidemic in 2019 has cast a great impact on people's lifestyles with the increased size and density of cities[2, 3]. There were 548 million infections confirmed worldwide by 1st July, 2022 with a total of 6.33 million deaths covering 215 countries and regions, causing a global crisis with profound social impacts[4]. On this basis, a large number of relevant studies on safe ventilation in large cities have emerged, especially in combination with the study on microbial aerosol (MA) diffusion pollution of the COVID-19 virus. Microbial pollution includes viruses, bacteria, mycoplasma, fungi or their spores adhering to air particles. Microorganisms suspend in the air in the state of a single cell and connect with dry solid particles and liquid particles, forming microbial aerosol which can spread to dozens of kilometers with the airflow[5, 6]. The study on the diffusion form of MA pollution can provide practical measures for the identification of high-risk groups, evacuation and resettlement of residentials during major public health security incidents, and the corresponding risk assessment will provide technical support for the optimization of urban ventilation schemes and the future urban architecture upgrading guidelines[5, 7].

Therefore, the study of urban ventilation mechanisms has become the scientific research frontier of key institutions worldwide with the spread of the COVID-19 epidemic situation[8]. The continuous revelation of the transmission mechanism of viral aerosol mainly contains the simulation model research[4, 9-11] and the project study[8, 12].

(1) In the field of simulation model research, simulation model selection and optimization are the main focus of computational fluid dynamics research[13]. Specifically, gauss floating calculation (SCIPUFF) was used in the fast 3D-CT model to reveal the propagation characteristics by ignoring the Lagrangian method of vortex shedding[14, 15]. The selection of the meteorological model under the typical LES model (mms/ obs) was also discussed [16] besides the parameters of air exchange rate and

reentry ratio[17]. Model optimization mainly contains non-CFD (Computational Fluid Dynamics) methods to solve the problems of large modelling costs[18], and replacement of 3D scenes with 2D simulation aiming at a low computational cost[19]. Studies have been made on the extraction of 13 ventilation indexes[8] from a total amount of 63 pieces of literatures in recent years as the direct monitoring parameters of the simulation study.

(2) In the field of project study, the main requirements are the large computing resources support interfacing with different computational models. Specifically, the combination of CFD and the Weather Research and Forecasting model (WRF) has been used to simulate the emergency public safety events in the Central Park in New York[20], while the combination of the Computational Fluid Dynamics (CFD) model with the chemical reaction model (CBM-IV) was also used[21]. The large-scale simulation of city security is getting more and more attention as the study on the diffusion path of pathogenic aerosol in Hong Kong[22]. Besides, the relatively small-scale simulation includes street canyon level and building level. The semi-empirical multi-layer model[23] has been established and the corresponding residential-industrial compatibility principles were analyzed[24] through urban canopy layer (UCL) research at the street canyon level. Aiming at the control of urban air quality, the diffusion of street traffic pollution in Beijing was revealed under the combined analysis of simulation and onsite testing[25], while three quantitative indicators were put forward to form the "urban permeability map"[26]. The diffusion pattern of traffic pollutants around buildings with plant belts was analyzed under simulation and experimental study[27], together with the impact of urban structure on the average air age at the building level[28]. The LES model with high-velocity spatial resolution[29] was used to study the influence of stable layered roughness sublayer on the transmission of scalar parameters to improve the details of the architectural design. Furthermore, gas and suspended particle pollutants[12] were studied and the intake fraction[30] was used to characterize the impact of ultra-fine particles on the human exposure of the indoor environment.

In conclusion, The research on the diffusion of urban pollution has become the frontier of research institutions around the world with the continued development of the COVID-19 epidemic situation[10, 31-36], containing wake coupling theory [37], wake vortex shedding phenomenon[30] and the disturbance of spatial building layout[13]. The current common research models have their suitable application scenarios. The SCIPUFF calculation ignores the phenomenon of residual vortex shedding to realize rapid reaction, while CBM-IV is more suitable for simulating the movement of specific fluid combinations with chemical reactions. Although the Semi Empirical Multi-layer model provides a convenient computing interface for the analysis of specific flow scenarios and can simplify the complex layered flow simulation, its core computing capability is limited by empirical calculation formulas., CFD calculation is still the most flexible, accurate and widely used calculation method at present.

However, two major problems still need to be further solved based on the existing research although research in this area has received widespread attention: (1) how to define the horizontal and vertical climate disturbance boundary on the basis of spatial dimensions to provide a clear and reliable scope for the urban planning and urban climate management in a quantitative way[22]. (2) how to clearly define the comprehensive risk assessment and pollution indicators caused by the public health security incidents to the living residents[17]. The comprehensive indicators need to reflect the spreading characteristics of pollution and the intensity of pollution transmission to provide an early warning of the residents' living safety after the emergency pollution break out[38], and also make an evaluation of the reliability of the building scheme at the beginning of urban construction[8, 12].

This study will take an Innovation Base under construction as the research objective to carry out a quantitative study on its urban design scheme relying on the CFD algorithm and onsite resting. The above problems on quick prediction of urban pollution diffusion and quantitative risk assessment of urban ventilation will be systematically explained to form: (1) aerodynamic characteristics analysis and numerical optimization scheme of the urban design, and (2) scientific measures for the

identification of high-risk groups, the evacuation and resettlement of residentials under epidemic prevention. Typical characteristics and effective control methods for the diffusion of COVID-19 are discussed. A series of design indicators containing the Amplification Coefficients on Urban Disturbance (ACUD), the Comprehensive Risk Coefficient (CRC) and the Comprehensive Pollution Disturbance (CPD) contribute to the design scheme facing quantitative urban ventilation evaluation and risk assessment based on traditional architectural design standards.

2 Methodology

The incipient design scheme was provided by the Shenzhen Institute of Building Science based on traditional architectural design standards. The building scheme and COVID-19 safety ventilation of the whole Innovation Base were analyzed with the specific monitoring points surfaces around the building combined with the first-order meteorological parameters and high-order flow parameters. The research is divided into simulation research, field study and modelling development. The simulation research was introduced to explore the detailed aerodynamic data of the ventilation environment in the Innovation Base, and then the on-site measurement of the field study was carried out to verify the simulation result. The field experimental measurement reveals that the field-measured data is in good agreement with the simulated data. Finally, the model deducing Amplification Coefficients on Urban Disturbance (ACUD), Comprehensive Risk Coefficient (CRC) and Comprehensive Pollution Disturbance (CPD) was carried out based on the detailed data export of the simulation to provide practical measures for risk assessment and epidemic control under the microbial aerosol pollution. The specific flow chart of the study on simulation research and field study is shown as follows in Figure 1.

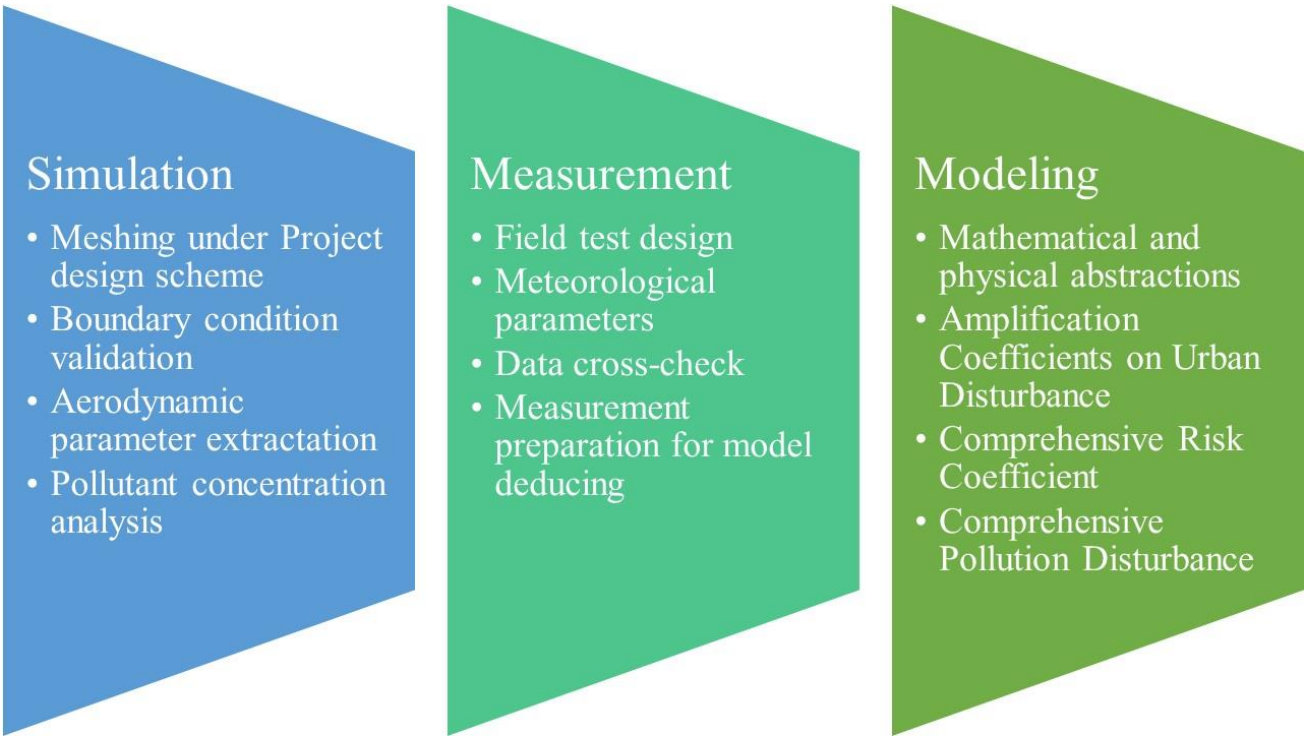

Fig. 1. Flow chart for the methodology containing Simulation, Measurement and Modelling

2.1 Project introduction

This work aims to study the mechanism and strategy of urban health ventilation based on COVID-19 aerosol pollution diffusion of the Sichuan-Chongqing Gaozhu Innovation Base, the overall planning is shown in Figure 2.

Fig. 2. The project demonstration of this study-Chongqing-Sichuan Gaozhu Innovation Base and the current construction progress

Sichuan-Chongqing Gaozhu Innovation Base was designed as the demonstration area for the integrated development of industry, city and scenery which integrates complex urban formats containing residential areas, commercial areas and industrial areas. Typical planning methods namely determinant, staggered, freestyle and enclosed building layouts are adopted integrating complex elements such as the interlocking skyline of podium and tower buildings, independent urban air ducts and mountainous terrain, providing an ideal research platform for the research of urban ventilation. Its abundant architectural layout forms and multiple functional areas, together with the

comprehensive production and living functions all contribute to a representative case study for the research. Basic information on the CAD model of the Innovation Base and the design for the onsite measurement is shown in Figure 3.

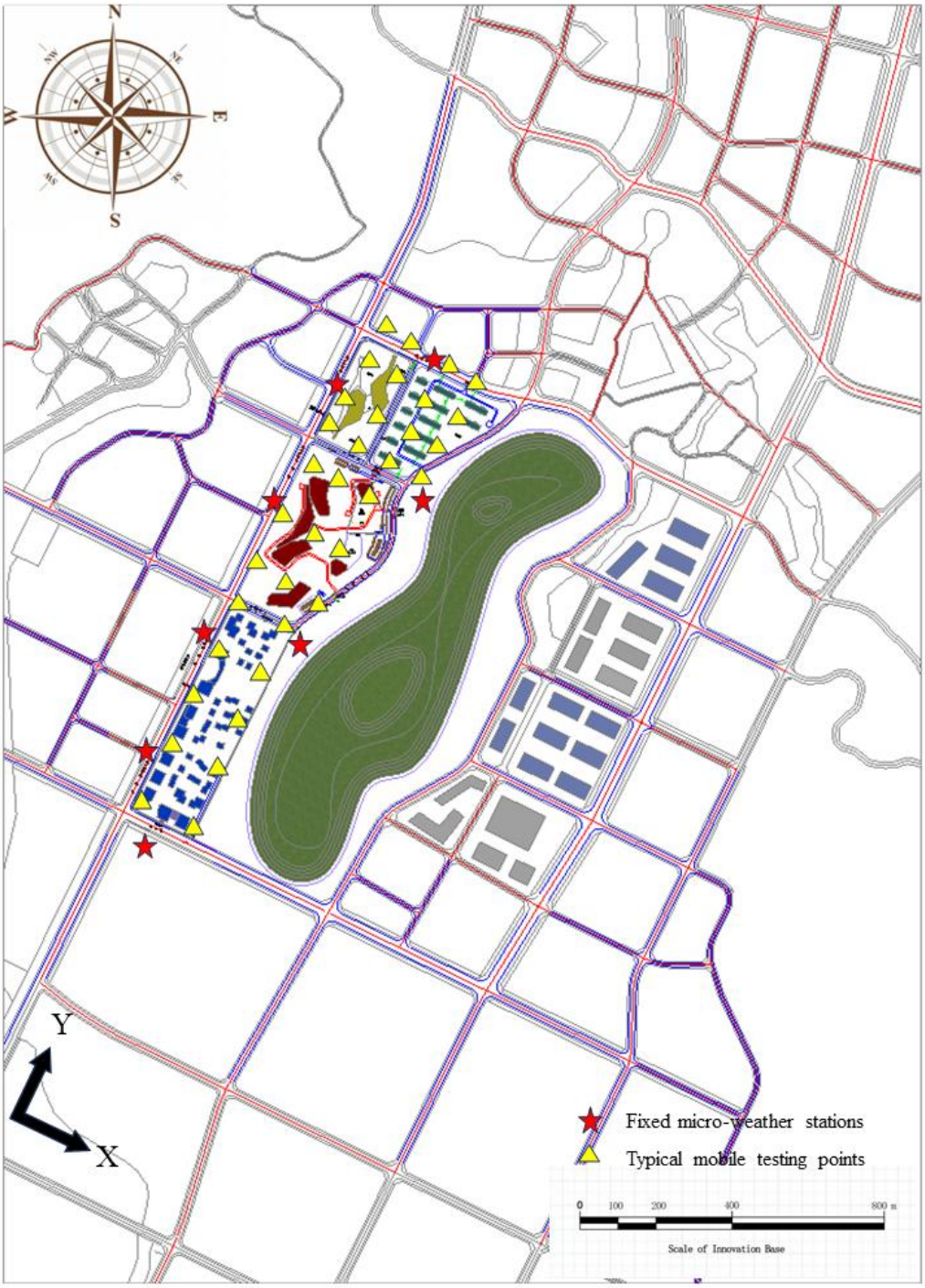

Fig. 3 CAD model of the overall planning scheme of the Innovation Base and the design for the following onsite measurement points based on Space Label Segmentation Methods[39]

2.2 Onsite testing introduction

This study relies on the experimental research platform of the School of Civil Engineering at Chongqing University to conduct relevant meteorological conditions and pollutant concentration testing onsite to achieve the following objectives: (1) explore the real meteorological boundary conditions through continuous monitoring of construction sites; (2) verify the accuracy of simulation research by monitoring key locations within the Innovation Base; (3) determine the boundary conditions for quantitative research on pollutant concentration. The onsite testing experimental instruments and testing scenarios are shown in Table 1 and Figure 4.

Table 1 The onsite testing experimental instruments

Instrument	**WWFWZY-1 Wireless Universal Wind Speed and Temperature Recorder**		**JTR04 wet black bulb thermometer**	**ppbRAE 3000 VOC detector PGM-7340**		**DUSTTRAK II aerosol monitor 8532**
Resolution	temperature wind speed	0.01 °C 0.01 m/s	0.1°C	± 3% of the calibration point for 10-2000 ppm isobutylene		± 0.1% or ± 0.001 mg/m³
Measuring range	temperature	-20 - 80 °C	-20~125°C	10.6 eV 9.8 eV	1 ppb-10,000 ppm 1 ppb 1 ppb-10,000 ppm 1 ppb	0.001 - 150 mg/m³
	wind speed	0.05 - 30 m/s		11.7 eV	0.1 ppm-2,000 ppm 10 ppb	
Calibration accuracy	temperature wind speed	± 0.5 °C 5% ± 0.05 m/s (0.05-30 m/s)	±0.5°C	Temperature range Humidity range	-20º C - 50 º C 0% to 95% relative humidity (non-condensing)	± 0.002 mg/m³ after 24 hours of use
Record time interval	2 sec - 24 hour		1 - 255 min		1 - 3600 sec	1 sec - 1 hour

The onsite testing of the study was carried out based on the experimental design scheme of the Chongqing Construction Science and Technology Plan (No. 20220184). The experiment design chose the month and days with the highest frequency of dominant wind direction of the Innovation Base according to the "Meteorological Database of Major Cities in China" of Tsinghua University. The onsite meteorological data testing method of the Ruifeng - Eling Project[39] was introduced in this study (the three-star certification of Green Building in China and Green-Mark Platinum Certification in Singapore, the highest level of Green Building Certification in both countries). The onsite experiment for this study has gone through 60 scenarios of field tests containing 8 fixed micro-weather stations for long-term environmental parameter monitoring and 35 typical mobile testing points selected from the field.

Fig. 4 The onsite testing scenarios around and within the Innovation Base

2.3 Model description

2.3.1 Computational domain

The building coverage area is less than 7% of the entire calculation domain according to the wind field simulation requirements, and the target building group is set in the center of the airfield. Parameter H1 is set as the longest horizontal length while H2 is set as the longest vertical length of the Innovation Base. The three-dimensional size in the XYZ direction is 7500 m, 13627 m and 600 m respectively according to the architectural design size of the Innovation Base.

2.3.2 Boundary conditions

In terms of meteorological boundary conditions, the natural gradient wind with an annual wind speed assurance rate of 10% is selected as the design boundary condition based on the special meteorological data set for thermal environment analysis of "Meteorological Database of Major Cities in China" of Tsinghua University[39]. The onsite meteorological data testing was carried out for the meteorological parameter verification and simulation result verification. The boundary conditions use the combination of velocity-inlet and pressure-outlet in the south and north direction respectively. The east, west and top surfaces of the air domain were defined as free slip with a shear-force of 0. Air floating particles at the average size of 10 μm with the normal distribution range of [1 μm, 100 μm] as the releasing source are created which COVID-19 attaches to.

2.3.3 Mesh modeling

The total number of mesh grids of the air domain is 33.69 million with 715 surfaces and 3127 curves, and 31.28 million tetrahedral cells. Element parts near the ground and the building group are densified as 2133263 and 17955 respectively to get higher accuracy in the key regions.

The mesh quality is also calibrated by the method of Equi-Size Skew. The best mesh quality is 0.99 while the worst is 0.10 accounting for 4.12% of the total mesh, with the average quality value of 0.74 and the most concentrated area of grid quality is [0.90, 0.95] accounting for 23.36%. The Grid sensitivity analysis and validation test were also carried out by an extra mesh under the same design scheme with a total element of 85.82 million.

2.3.4 Calculation settings

This simulation was carried out on the pressure-based model under transient calculation. The gravity and temperature field are coupled during simulation while the multi-component model and discrete phase model have interacted. The standard k- ε model is selected for turbulence combined with

Lagrange diffusion mode to ensure the simulation accuracy of particle migration. The residual monitors of continuity and energy were defined at $1*10^{-3}$ of $1*10^{-6}$ respectively for convergence.

The building design scheme was analyzed on two surfaces referring to China Green Building Standard (GB/T 50378-2019): (1) the outdoor pedestrian activity region, 1.5m high plane above the ground, and (2) the building window ventilation region, 0.5m offset from the building facade. A total of 35 surfaces of pollution source corresponding to the exhaust outlet, pedestrian entrance and exit based on the building scheme were picked out by the official construction company of the Innovation Base "Sichuan Provincial Investment Group Company Limited", where pollution was prone to occur according to the existing design scheme as shown in Figure 5, together with the mesh image of the total calculation domain. The comprehensive information of the simulation study is presented in Table 2 based on the current study on urban ventilation[40, 41].

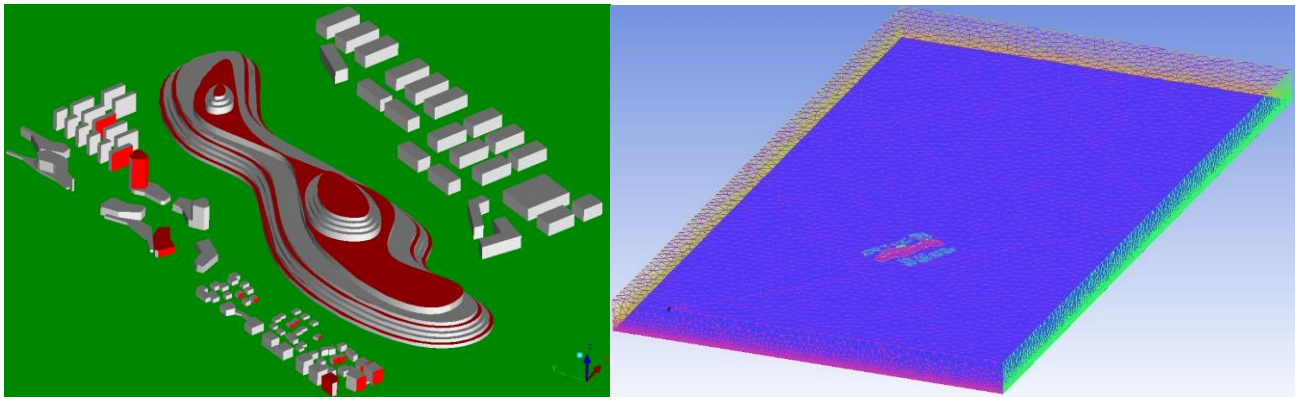

Fig. 5 Extraction of typical pollutant diffusion source in the building design scheme shown in the red plane in the figure and the mesh image of the total calculation domain

Table 2 Comprehensive information of the simulation study

Items	**Distribution**		
Domain	Length	Width	Height
	13627m	7500m	600m
Geometry	Elements	Surfaces	Curve
	3369	715	3127

Quality	Average value			Maximum value			Minimum value	
	0.74			0.99			0.10	
Particle	Average diameter			Maximum diameter			Minimum diameter	
	10μm			100μm			1μm	
	Distribution function							
	$f(x) = \frac{1}{\sqrt{2\pi}\sigma}\exp\left[-\frac{(x-\mu)^2}{2\sigma^2}\right]$							
Boundary		Temperature		Velocity inlet	Pressure outlet		Wall	
	Air	Ground	Building	South	North	East	West	Top
	28℃	30℃	32℃	Natural gradient	Far-field	Smooth wall	Smooth wall	Smooth wall

3 Result

3.1 Morphological characteristics of COVID-19 distribution

It is necessary to extract the vortex structure by certain methods to research the vortex structure of turbulence, where we introduce the definition of vortex core. The vortex core in this study was extracted under the method of "Q" which represents the second-order invariant of the velocity gradient ∇U. The detailed definition is as Equation 1 to Equation 5.

Eq. 1 – Eq. 5:

$$Q = \frac{1}{2}(\|W\|^2 - \|S\|^2)$$

$$W = \frac{1}{2}[\nabla U - (\nabla U)^T]$$

$$\|W\| = (W{:}W)^{1/2}$$

$$W = \frac{1}{2}[\nabla U + (\nabla U)^T]$$

$$\|S\| = (S{:}S)^{1/2}$$

The formation of a vortex core around the building is the intuitive embodiment of the turbulence formed under the impact of airflow as shown in Figure 6. The location of the vortex core provides basic reference criteria for greening design and building overhang design for the architectural scheme. A vortex core with a maximum speed of nearly 5 m/s is formed around the highest building of the Innovation Base on the windward side indicating the intensity of the wind speed field formed around the building.

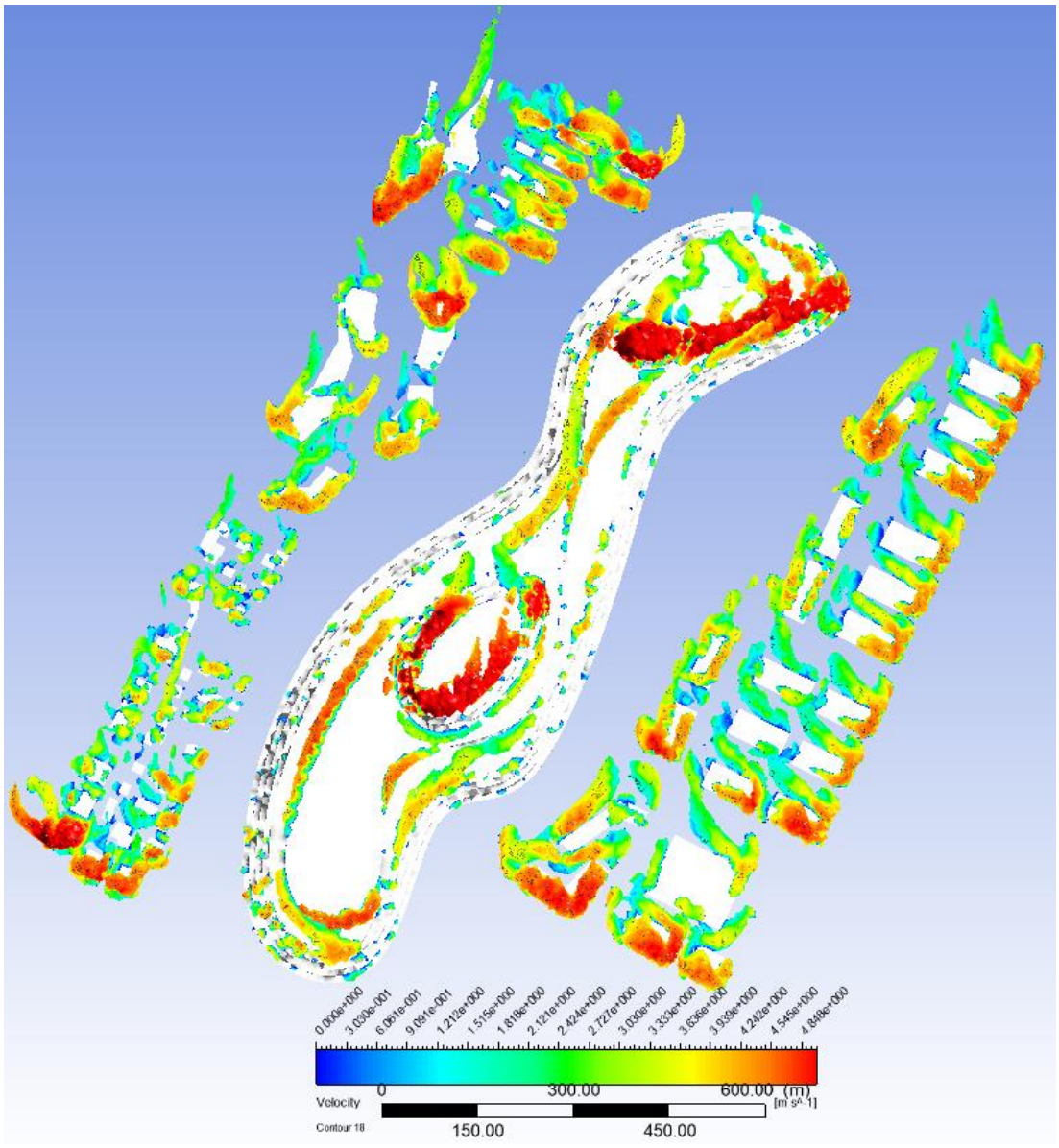

Fig. 6 Distribution of velocity nephogram of vortex cores around buildings

This study uses a vortex shell to capture the COVID-19 virus diffusion route and intensity as shown in Figure 7. The results showed that the virus particles were concentrated in the vortex shell with a

concentration of COVID-19 around [0,10^{-6} kg/m^3] which is three orders of magnitude lower than the initial releasing concentration at 1.67*10^{-3} kg/m^3. The COVID-19 particles concentrate around the releasing building facades with the development of the vortex shell under natural meteorological conditions, within 20 meters around the building according to the vortex nephogram. The hypothesis on one absolute COVID-19 infection was not adopted in this study, and it is not simply considered that a person is infected when a single virus appears. The concept of "particle mass concentration" was introduced in this study based on the "Chongqing Municipal Postdoctoral Research Flow Project Special Grant (No. 2211013357670761)". The COVID-19 virus attaches to the surface of particles suspended in the air with a normal distribution, and will cause high-risk human infection when the particle mass concentration rises above 1.0*10^{-6} kg/m^3 in this study.

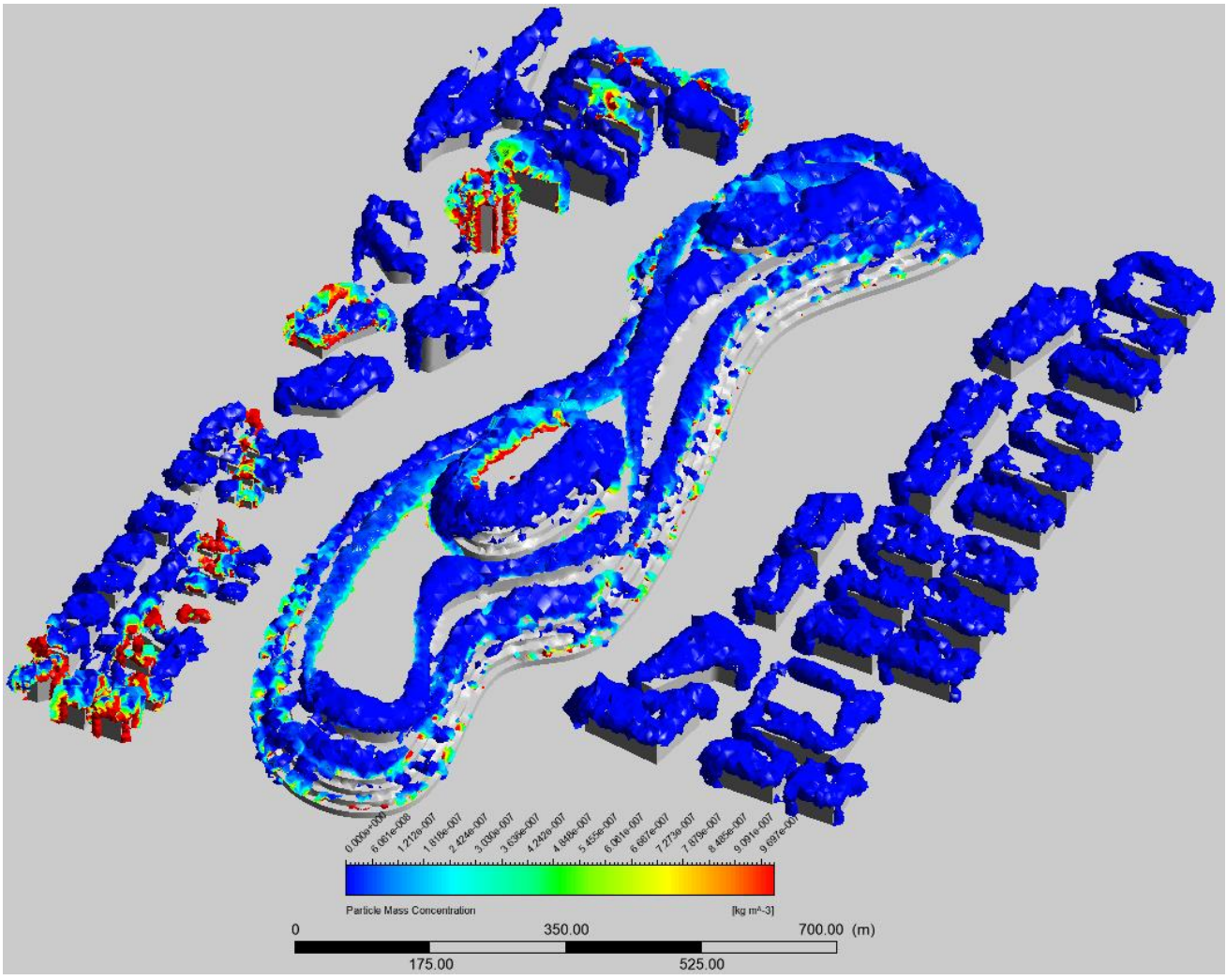

Fig. 7 Distribution of COVID-19 particles with vortex shell around buildings

3.2 Onsite testing and verification on simulation

The actual meteorological conditions and the particle concentration from the working dust on the construction site during the testing period are used as input boundary conditions for the comparative simulation experiment. The 10 monitoring points were selected in the 3D-model space to compare with their measured data of the corresponding monitoring points on site. The comparison of the simulation result and the onsite testing are shown in Figure 8. The simulation calculation results showed good agreement with the onsite test results for the typical environmental parameters (wind speed, pressure) and particle concentration. The simulation results show consistent changes in both trend and numerical magnitude with the onsite testing results indicating the simulation represents the ventilation scenario. The specific experimental test data are shown in Figure 8.

Fig. 8 Comparison of the data of the simulation result and onsite testing of corresponding monitoring points where the X axis represents the type of test data and the Y axis represents the data value

This study introduced the Pearson Correlation Coefficient to analyze the parameters in Figure 8 to reflect the quantitative index of simulation accuracy. In statistics analysis, Pearson Correlation Coefficient, also known as Pearson Product-Moment Correlation Coefficient (PPMCC or PCCs), is used to measure the correlation between two variables X and Y. A value of 0 means that there is no correlation between the two variables, and the closer the coefficient is to 1, the better the correlation relationship is between the data. The Pearson Correlation Coefficient of the parameters is calculated, showing that the PCC of the pressure, velocity and particle concentration are 0.9853, 0.8755 and 0.9856 respectively, representing a good correlation between the result of the simulation and onsite study.

4 Discussion

Numerical research on the building scheme can be divided into two aspects: (1) study on the aerodynamic characteristics of the horizontal wake area of buildings. Existing studies have shown that the building wake area is not only the high incidence and concentration area of air pollutants, but also the formation area of eddy currents in large urban building clusters. The interference between wake streams endangers the residential safety of downstream residents. (2) study on the vertical ventilation potential of urban canopies. The purposes of urban air duct design are to improve the ventilation capacity of the city and to quickly discharge the polluted air generated by the city among which the vertical emission at the street canopy level is currently considered to be the most effective way. The key research areas containing the pedestrian plane (1.5m from the ground) and the building ventilation surface (0.5 m from the building facade) are studied to analyze the concentration distribution characteristics of the COVID-19 pollutants. The three-dimensional disturbance boundary of the building complex on the development of the entire urban wind field at the spatial level is discussed.

4.1 Horizontal disturbance of urban ventilation

The plane 1.5m above the ground is analyzed to study the distribution characteristics of the

pollutants with meteorological parameters. The scope of the wake area on the leeward side of the buildings is defined as shown in Figure 9 showing that the leeward side of the buildings has met the rapid pressure drop region within the range of Y= [0, 20] and an obvious negative pressure area appeared in this region due to the influence of the horizontal pressure gradient force on the airflow. The pressure is gradually increases due to the appearance of the internal primary vortex boundary within the range of Y= [20m, 70m]. The wake of the building group is formed and the pressure gradually reduced to 0 When meeting the breakdown of the primary vortex within the range of Y= [70m, 2800m].

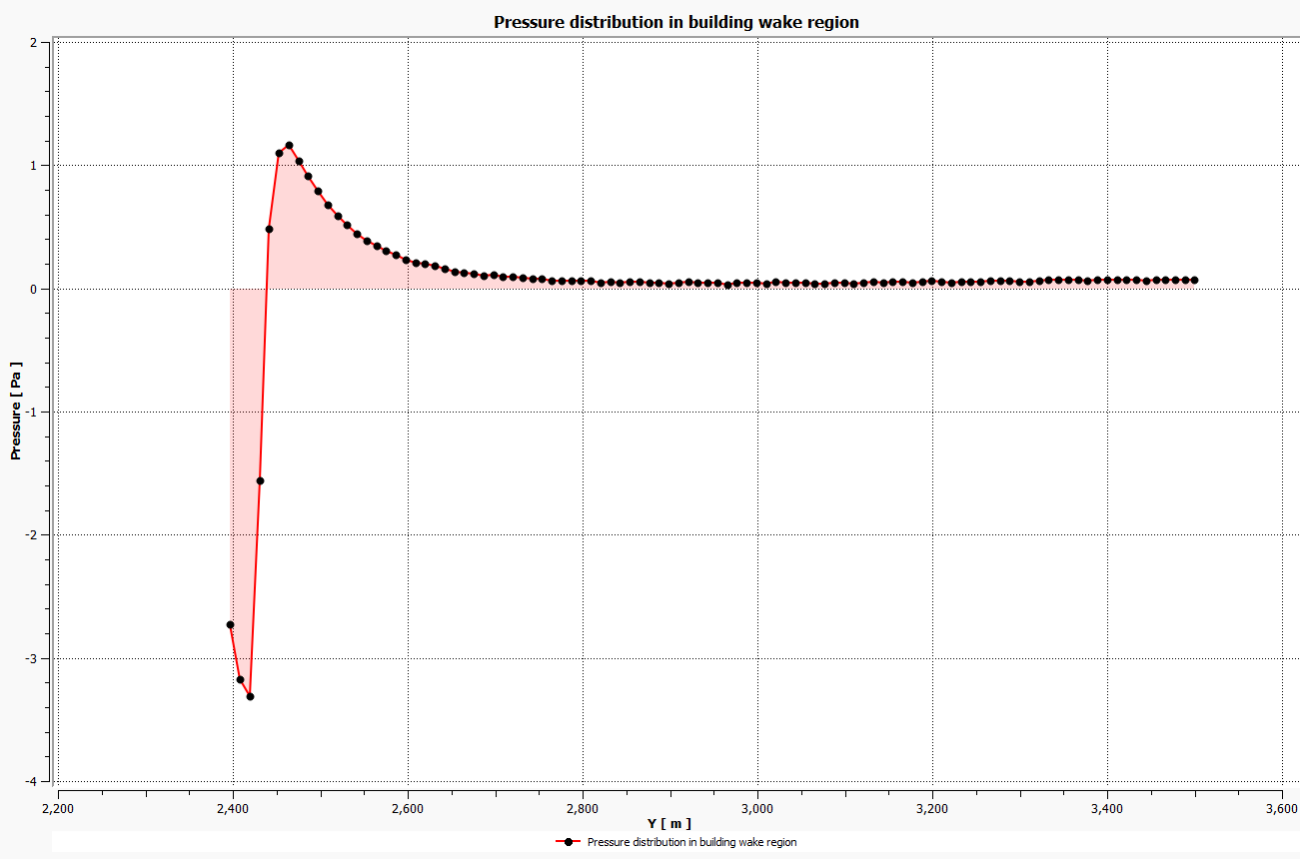

Fig. 9 Pressure distribution in the wake area on the leeward side of the building group where the X axis represents the distance from the building façade in the Y direction and Y axis represents the pressure

The leeward side here refers to the large vortex wake area formed by the Innovation Base in the direction of the wind, which causes not only natural gradient wind disturbance, but also the gathering of pollutants, making it becomes the focus of modern urban planning research. The practical

significance of the study on the large vortex wake area lies in the influence of the urban landscape formed by the building groups on their downstream urban regions, to determine the disturbance range of the building groups on the urban ventilation, or the retreat of the downstream buildings during the urban design.

4.2 Vertical disturbance of urban ventilation

The 3D streamlines of 5000 clusters are established for the parameter variables captured in the whole air domain. The corresponding velocity decomposition of airflow in the direction of height and horizontal airflow is shown in Figure 10. The selection of 3D streamlines of 5000 clusters is to capture the fluctuation characters and the changing parameters on the streamlines from a spatial scale. The amount of data is large enough which can well reflect the parameter fluctuation at different locations in the space based on the final performance. The location of the urban boundary layer (UBL) and canopy layer (UCL) can be qualitatively identified through the vertical decomposition of air velocity. Due to the disturbance of the urban building boundary layer, the decomposition U_v of wind speed in the horizontal direction is distributed within the range of height Z=130 m under the UBL boundary. The disturbance of the urban boundary layer UBL to the natural gradient wind will be terminated and the natural gradient wind will return to the exponential distribution when the height reaches Z=300 m. Meanwhile, the irregular disturbance scatter distribution of U_w is concentrated within Z=130 m. The U_w stratification is higher than Z=130 m due to the eddy current combined with the building plume at the top of the building. The U_w shows an exponential gradient attenuation to 0 under the interaction of natural gradient wind when the height exceeds Z=300 m.

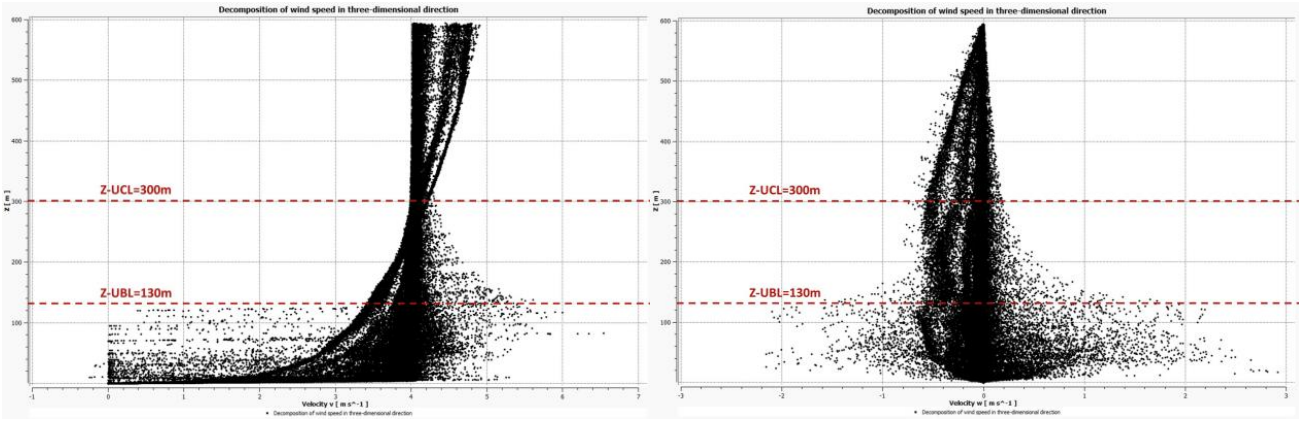

Fig. 10 Distribution characteristics of air velocity decomposition in the vertical and horizontal direction where the X axis represents the velocity decomposition and the Y axis represents the height

The space size of the primary vortex zone is small and the parameters change sharply resulting in serious pollution. The spatial size of the secondary vortex zone is large and the meteorological parameters are smaller compared to that of the primary vortex zone. However, it is difficult to carry out direct measurements on the region definition of vortex in practical applications due to their small changes in parameter values and directions. Thus, it is of great significance to divide the first-order and the second-order eddy current influence range of the building cluster by an accurate evaluation method. The following part of the research will establish a serious of design indicators in combination with the simulation method to the define of primary and secondary vortex zones accurately.

4.3 ACUD analysis in the horizontal direction

Further study on the fluctuating characteristics of aerodynamic parameters under shield turbulence is carried out based on the measurable meteorological parameters. the absolute value of typical aerodynamic parameters is controlled within the range of [0, 2.5] through a unit transformation to facilitate comparative analysis as shown in the Figure 11. The typical extreme points appear at the spatial distance of Y=4 and Y=8 through the observation of TED/TKE/V/V_v/WS and the corresponding spatial distance is ΔY=60 m and ΔY=120 m respectively. The TKE and TED decrease rapidly due to the direct influence of wind speed within ΔY=60 m forming the first-order vortex zone

behind the last row of buildings. The first-order vortex at ΔY=120 m breaks under the effect of space turbulence and TKE gradually increases to a stable state. The flow aerodynamic parameters begin to oscillate when the distance is further increased to Y=37, that is ΔY=520 m.

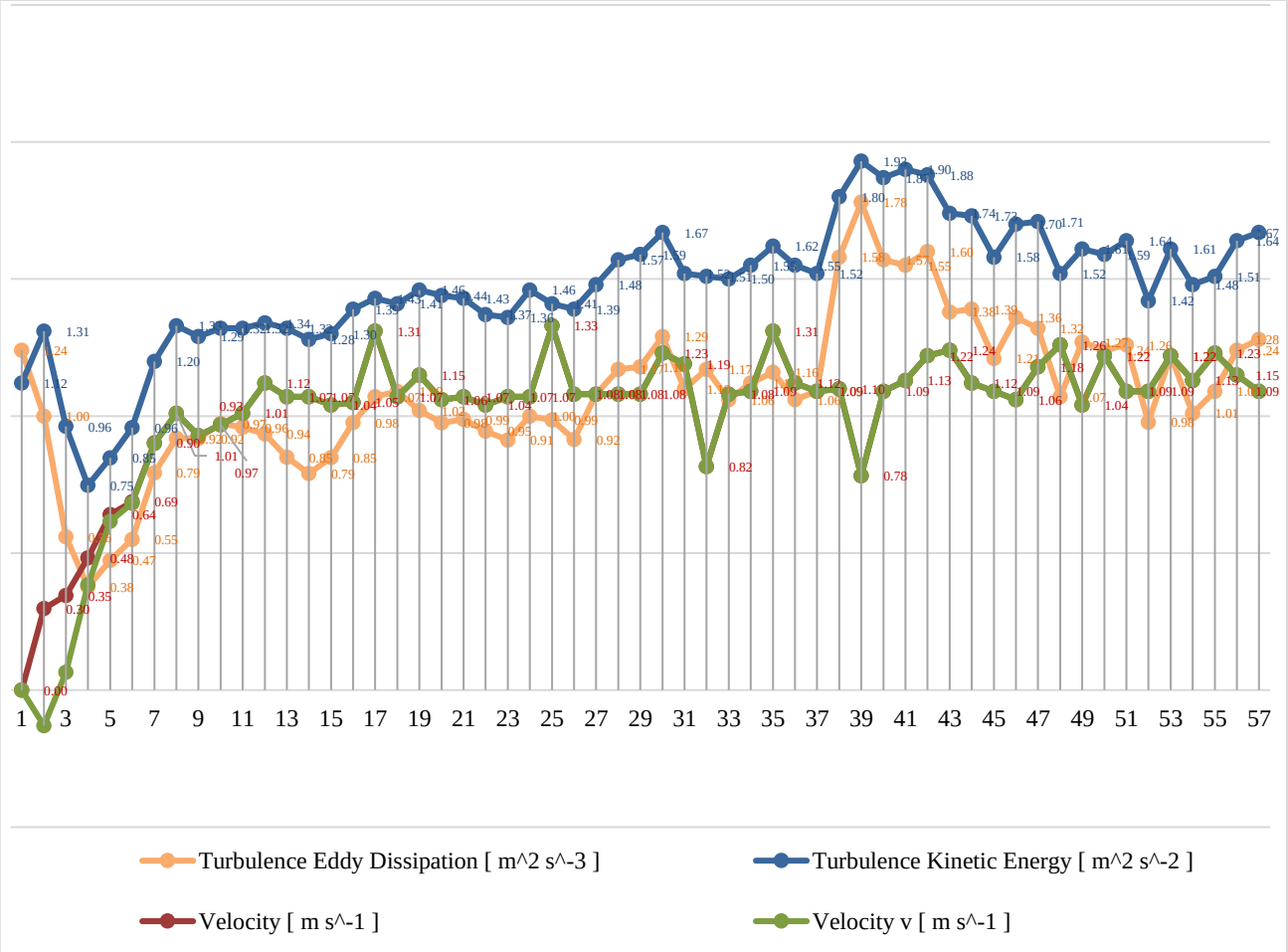

Fig.11 Fluctuation of the first-order aerodynamic parameters on a pedestrian plane in building wake area where the X axis represents the distance from building façade in the Y direction and Y axis represents the parameter variation

The aerodynamic parameters of the first-order vortex are further expanded as shown in Figure 12 based on the above conclusions. It is further found from the figure that the concentration of pollutants decreases rapidly when Y=2 (ΔY=30 m). The concentration of virus particles decreases rapidly due to their Brownian motion after release from the pollution source and the virus diffusion fluctuates rapidly due to the disturbance of airflow. At the same time, the TED_G reaches the minimum value at ΔY=60 m, when the corresponding EV_G and TKE_G also reach their minimum where the first vortex formed in the wake area of the building finishes.

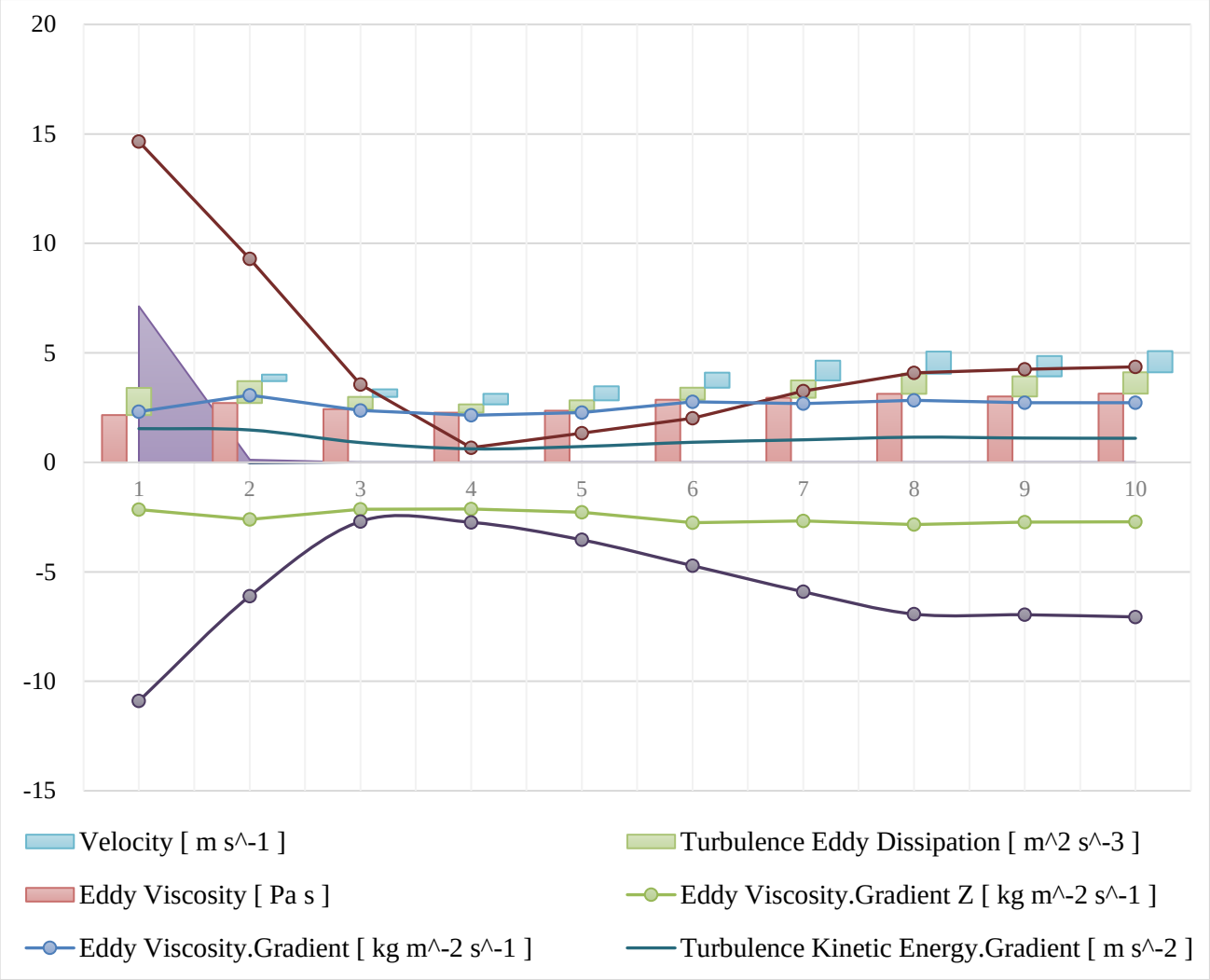

Fig.12 Distribution of low and high order aerodynamic parameters on pedestrian plane in building wake area where X axis represents the distance from building façade in Y direction and Y axis represents the parameter variation

In conclusion, the length of the building wake region under this design scheme is 1290 m along the wind direction, so the typical boundary is obtained on (1) ΔY=60 m, the length of the first-order vortex formed in the horizontal direction of the wake area, (2) ΔY=120 m, the transition length from the first-order vortex to the second order vortex, and (3) ΔY=520 m, the finishing length of the second-order vortex.

The amplification coefficients of urban disturbance in the wind speed direction of the Innovation Base reach σ_1=0.047 representing a high pollution concentration area and safe evacuation distance for ventilation of new buildings in the downstream direction), and σ 2=0.403 representing a low

pollution concentration area and ventilation quality retreat of new buildings.

4.4 ACUD analysis in vertical direction

Urban Street Canyon is an important channel for urban sewage discharge and space purification. The study of aerodynamic parameters of the street canyon can define the urban boundary layer to further propose specific requirements on the height of new buildings in the building cluster. On the other hand, the height of urban canopy which plays an important role in urban meteorological research and urban canopy pollution control can be quantitatively described. The monitoring line of [0, 600 m] in the height direction of the interval Z is established at the geometric center of the street canyon under the current building scheme. The low-order and high-order aerodynamic parameters of the street canyon are studied.

The distribution characteristics of EV/TED/TKE/P in the street canyon are shown in Figure 13. The maximum negative pressure area is generated and the urban boundary layer reaches its pressure boundary when Z=21 or ΔZ=126 m. The urban ventilation passes over the sharp edge of the tallest building when the upward building plume and the horizontal wind together form a first-order vortex. The typical aerodynamic parameters as EV/TKE/TED have met the obvious deflection when the altitude continues rising to Z=73 or ΔZ=438 m. The disturbance of the building is over and the boundary of the secondary vortex zone appears under the influence of natural gradient wind. Furthermore, the high-order aerodynamic parameters produce gradient mutation when the height continues to rise, and the aerodynamic parameters have experienced sudden changes in the gradient direction when the height continues to rise to Z=47 or ΔZ=282 m based on the gradient analysis of the extract data in Figure 13. The stable flow field in a certain space above the roof is gradually destroyed under the influence of natural gradient wind and the high-order aerodynamic parameters gradually transform into natural gradient wind.

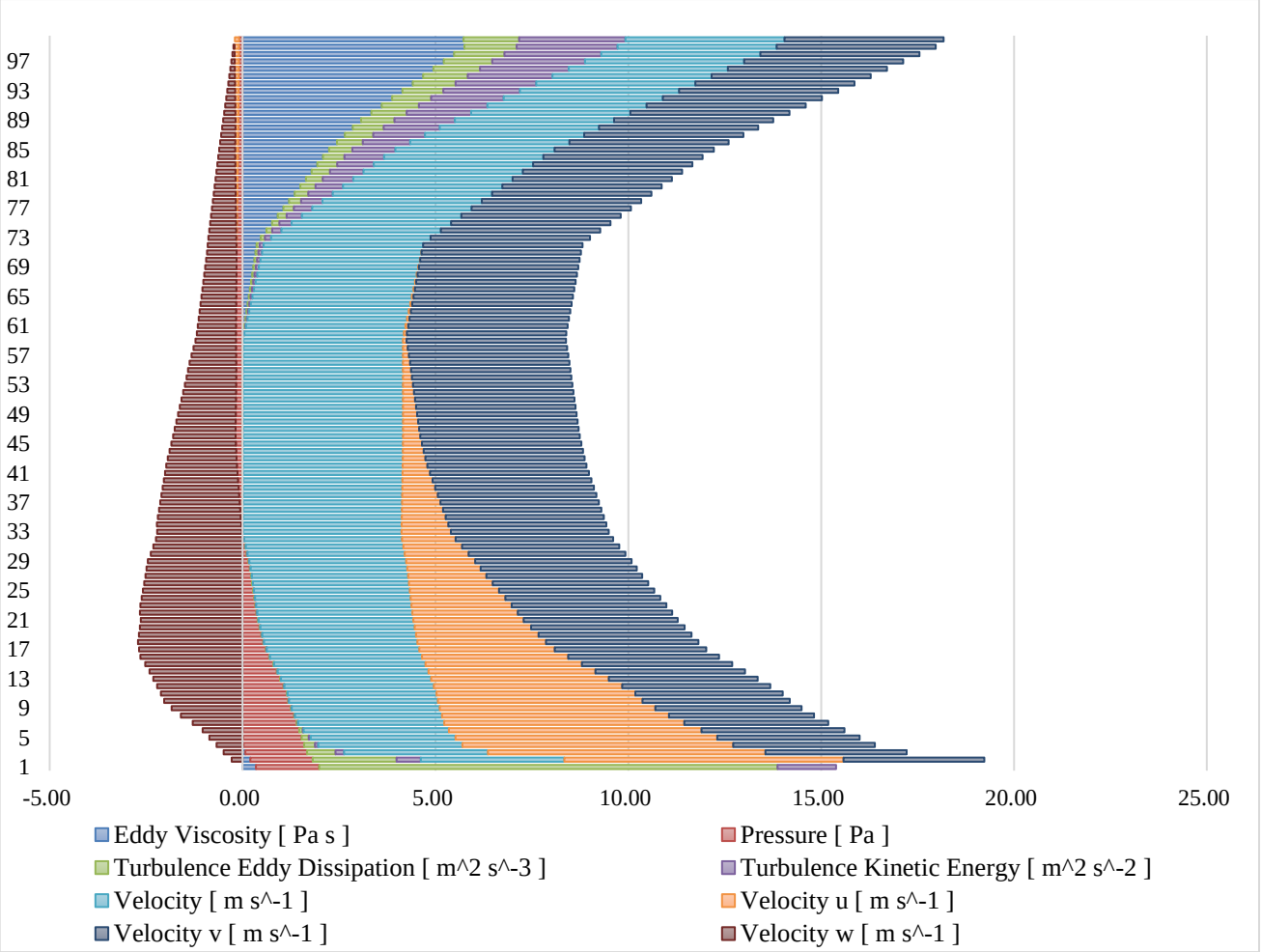

Fig. 13 Distribution of low-order aerodynamic parameters of street canyon in the Innovation Base where the X axis represents the parameter value and the Y axis represents the height

In conclusion, the maximum building height of the design scheme is Z=99.9 m, so the typical boundary is obtained at ΔZ=126 m, ΔZ=282 m and ΔZ=438 m corresponds to the amplification factor. The corresponding values are: (1) the height of the first-order vortex formed in the height direction, (2) the transition height from the first-order vortex to the second-order vortex, and (3) the finishing height of the second-order vortex. The Amplification Coefficients are defined as the disturbance magnitude of the natural wind by the presence of building groups of a certain size in a particular urban area. Specifically, it represents the ratio between the extension distance of the vortex boundary of the airflow generated by the building group and the size of the building group (the length, width and height of the building group) in different directions as shown in Equation 6:

Eq. 6:

$$\sigma_{AC} = \frac{\Delta L_{air}}{\Delta L_{building}}$$

The Amplification Coefficients of urban disturbance in the height direction of the Innovation Base are respectively σ_1=1.26 representing the control range of the skyline of new buildings, and σ_2=4.38 representing the urban canopy ventilation boundary.

5 Mathematical Model for Risk Assessment

The main concern in practical application is the distribution of pollution on the contact surface of people in horizontal and vertical directions in case of public safety incidents in the building complex, focusing on (1) the expansion and irregular distribution of pollution area, and (2) the random and uneven distribution of pollution intensity.

Therefore, this study determines the pollution contact plane and provides quantitative evaluation indicators for the corresponding pollutant concentration. Firstly, the monitoring of COVID-19 particle concentration and contaminated area percentage was carried out on the pedestrian plane of 1.5 m above ground in the horizontal direction. Secondly, the windowed ventilation area of 0.5 m offset from the building facade was chosen as the research area in the vertical direction, and the pollutant concentration and contaminated area are monitored simultaneously. The results were shown in the Figure 14 (a) and Figure 14 (b).

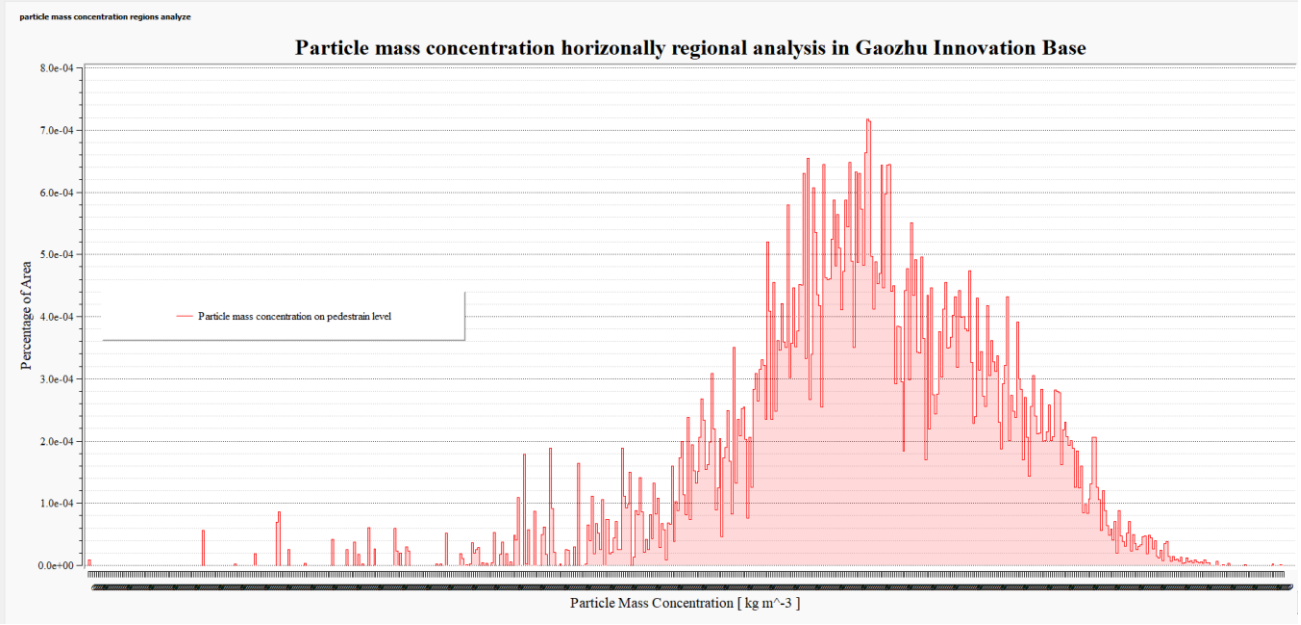

Fig.14(a) Particle mass concentration horizontally regional analysis in Gaozhu Innovation Base where the X axis represents the particle mass concentration and the Y axis represents the percentage of area

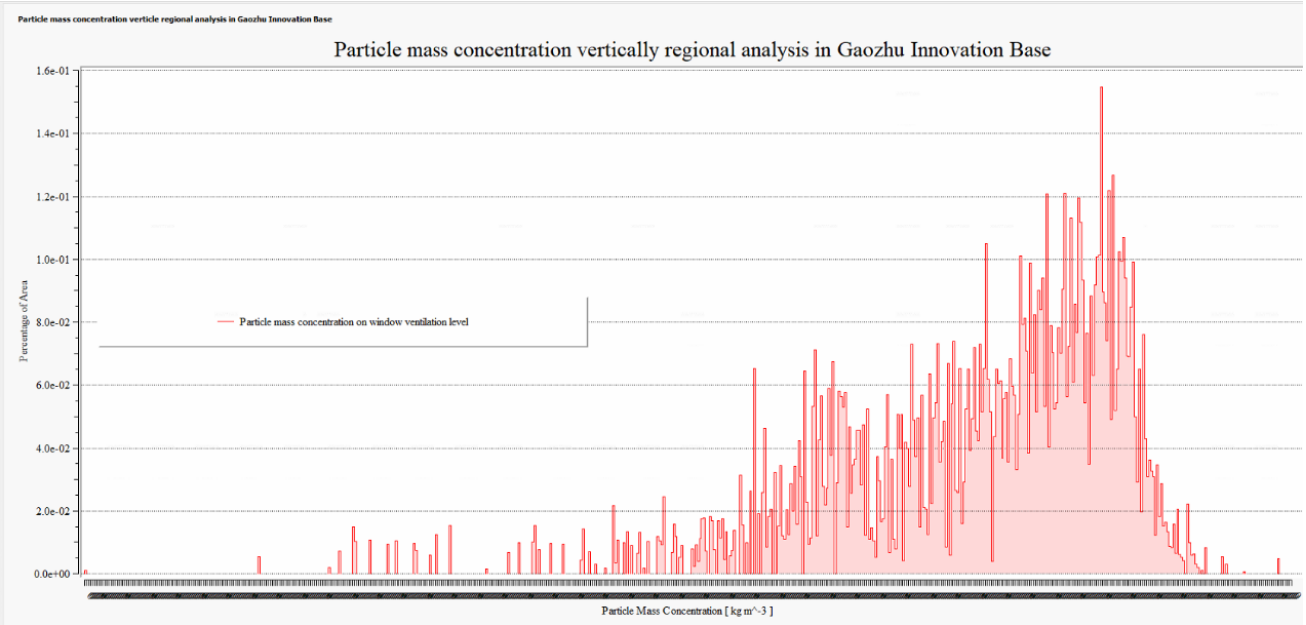

Fig.14(b) Particle mass concentration vertically regional analysis in Gaozhu Innovation Base where the X axis represents the particle mass concentration and the Y axis represents the percentage of area

The COVID-19 particles show complex uneven distribution in space and intensity in both horizontal and vertical directions as shown in the above figure. This unbalanced distribution can be understood as the distortion in both spatial distribution and mass distribution due to the outbreak of pollution.

Thus, the concept of the centroid system is introduced in the following part to research the distortion of the above two dimensions

5.1 Comprehensive Risk Coefficient

The concentration of pollutants on the surface of the Innovation Base can be measured and justified at the same time. Those who enter the Innovation Base at random will be affected by (1) the risk of pollutant concentration, and (2) the risk of pollution range where they are located. Therefore, it is necessary to make an abstraction on the two elements of random area and random concentration when studying the risk of human infection.

The hypothesis is made that there is an ideal plane galaxy P_g with a fixed boundary in space, the total area of the plane galaxy is 1 unit, and the total mass is also 1 unit. The ideal galaxy P_g is filled with equally divided stars with the same size ΔS_i, corresponding to the same planet density ρ. Then each planet occupies 1/n unit area and 1/n unit mass as shown in Equations 7 and 8:

Eq. 7:

$$n * \Delta S_i = 1$$

Eq. 8:

$$n * \rho * \Delta S_i = 1$$

However, the stars in the ideal plane galaxy P_g are in the process of free random growth in space, and their respective positions form different planets occupying areas S_1, S_2, S_3... S_i... S_n, and different planet densities ρ_1, ρ_2, ρ_3… ρ_i…ρ_n, corresponding to different masses M_1, M_2, M_3... M_i... M_n. The boundary of the galaxy P_g has been fixed, resulting in the random increase or decrease of the occupied area S_i of the individual planet P_i while the density of the individual planet ρ_i increases, as shown in Equations 9 and 10:

Eq. 9:

$$\sum_{i=1}^{n} S_i = 1$$

Eq. 10:

$$\sum_{i=1}^{n} Mi = \sum_{i=1}^{n} S_i * \rho_i > 1$$

At this time, an alien planet P_e (M_{Pe} =1) will be randomly and mistakenly inserted into the plane galaxy P_g after variation, and P_e will be constrained to the gravitational action of M_1, M_2, M_3... M_i... M_n. The gravitational effect of the mutated plane galaxy P_g on the alien planet P_e symbolizes the double disturbance of P_g on P_e in space and mass. The alien planet P_e is disturbed by the capture of a nearby planet P_i, which can be expressed as Equation 11 and 12 where C represents constant value.

Eq. 11:

$$F_i = G\frac{M_i}{r^2} = C * S_i * \rho_i$$

Eq. 12:

$$\sum_{1}^{n} F_i = \sum_{1}^{n} C * S_i * \rho_i$$

Different planets on the site of the grid areas S_1, S_2, S_3... S_i…S_n increases and decreases after galaxy variation while maintaining the total area of 1 unchanged, and the corresponding mass M_1, M_2, M_3... M_i... M_n in different grids S_i is differentiated. The summation of the perturbations of each planet P_i to the P_e of the alien planet is the comprehensive effect of the galaxy P_g to P_e. The ideal space plane galaxy P_g has become P_g' due to its internal mass and space evolution because of the random location

of P_e entering P_g. The gravitational field of the alien planet P_e is mathematically abstracted as P_g' gravitational field in the following function F (x) in Equation 13.

Eq. 13:

$$F(P_e) = \sum_{i=1}^{n} G\frac{\rho_i S_i}{{r_i}^2} = \sum_{1}^{n} H\left(\frac{\rho_i S_i}{{r_i}^2}\right)$$

The independent variable of function H(x) is transformed to eliminate the influence of the different dimensions on ρi, Si, and ri: (1) the $\rho_i * S_i$ is subject to a standardization process, because a single COVID-19 virus invasion can be identified as infection risk after the outbreak of a virus health event. (2) based on this standardization, the dimensionless sample eigenvalue variation coefficient CV, skewness SKEW, and kurtosis KU are introduced to replace the standardized centroid system and determine the mapping accordingly[42], related Equations are shown as follows.

Eq. 14:

$$CV = \frac{\mathrm{SD}}{\mathrm{AV}}$$

Eq. 15:

$$SKEW = \frac{\mathrm{n}}{(n-1)(n-2)}\sum\left(\frac{x_i - AV}{SD}\right)$$

Eq. 16:

$$KU = \frac{1}{\mathrm{n} * \mathrm{SD}^2}\sum_{i=1}^{n}(x_i - AV)^4 - 3$$

Eq. 17

$$f(r^2) = g(CV^2 + SKEW^2 + KU^2)$$

Therefore, the above formula can be transformed into the I (x) function in Equation 18.

Eq. 18:

$$F(P_e) = \sum_{i=1}^{n} I\left(\frac{Nor(\rho_i S_i)}{(CV^2 + SKEW^2 + KU^2)_\rho + (CV^2 + SKEW^2 + KU^2)_S}\right)$$

The above Eq. 18 can be converted into the following when extracting the corresponding concentration D_i and percentage area P_{ci} of COVID-19 particles as Equation 19.

Eq. 19:

$$\sum F(x) = \sum_{i=1}^{n} H\left[\frac{Nor(D_i P_{ci})}{\left(CV_{D_i}\right)^2 + \left(CV_{P_{ci}}\right)^2 + \left(SKEW_{D_i}\right)^2 + \left(SKEW_{P_{ci}}\right)^2 + \left(KU_{D_i}\right)^2 + \left(KU_{P_{ci}}\right)^2}\right]$$

In conclusion, based on the above abstraction, introduction and derivation, the flow chart for the calculation process and parameter introduction of the Comprehensive Risk Coefficient (CRC) development is shown in Fig. 15.

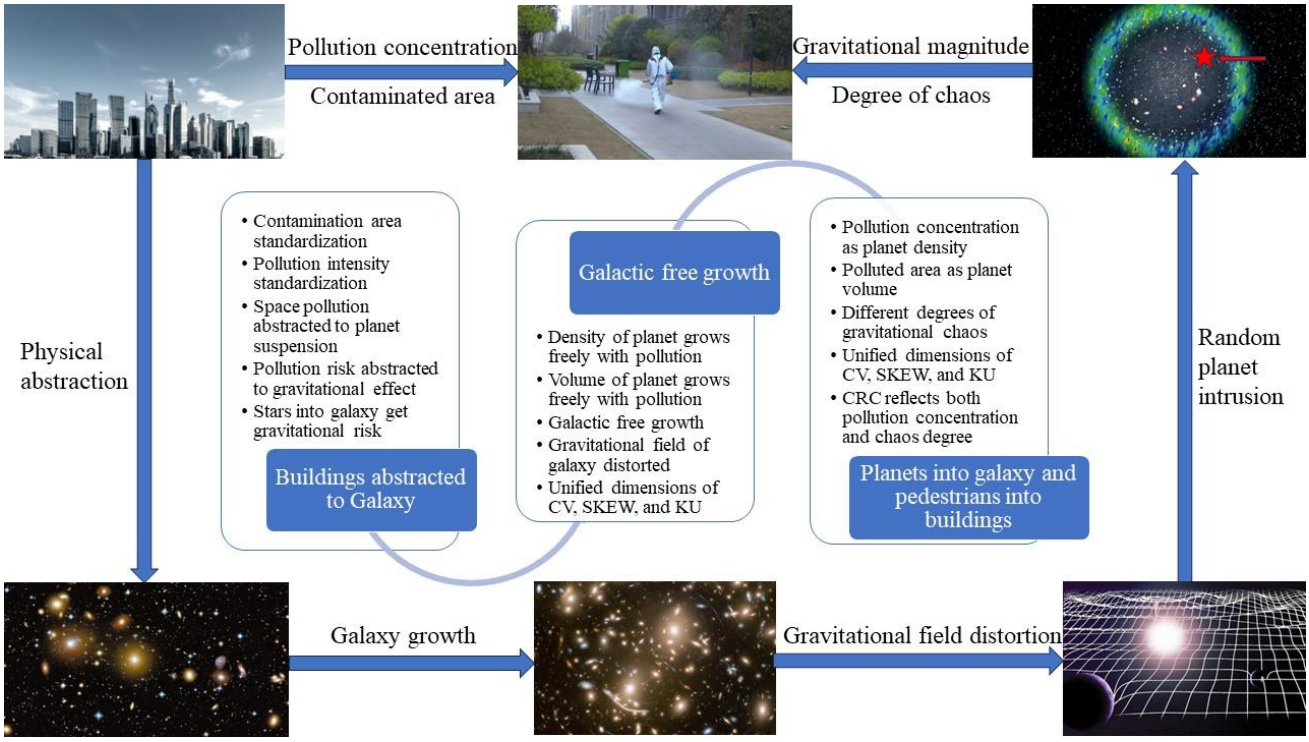

Fig. 15 Flow chart for the calculation process and parameter introduction of the Comprehensive Risk Coefficient (CRC) development (Pictures from the Internet, www. Baidu.com)

The Comprehensive Risk Coefficient is formed by spatial variables and concentration variables when an individual enters the irregular centroid system P_g randomly. In this case, the data of D_i and Pc_i in the plane 1.5m above the ground are substituted. The Comprehensive Risk Coefficient (CRC) in the horizontal direction is CRC_h=17.88, and the Comprehensive Risk Coefficient in the vertical direction is CRC_v=102.97. The risk of infection of personnel on the vertical contact surface is 5.76 times greater than that on the horizontal contact surface once the public safety event of the COVID-19 virus spreads in the building cluster. The CRC coefficient can also be applied to the infection risk assessment of other specific planes and points under the current building design scheme.

5.2 Comprehensive Pollution Disturbance

Health damage caused by different intensities of pollution should also be paid attention to when the concentration of pollutants is superimposed in practical applications, such as chemical pollution, nuclear pollution and some biological pollution.

There are two spatial distortions of pollution concentration and pollution area on the horizontal and vertical research planes which can be expressed by the introduction of Matrix Exterior Product decomposition. Matrix is a tool in advanced algebra which is mostly used in applied mathematics such as statistical analysis. The matrix is also usually applied in circuit science, mechanics, optics and quantum physics in modern physics study, specifically, an infinite matrix was used to deal with spatial distribution in planetary theory and atomic theory. The operation of the matrix can be simplified by the decomposition of the matrix into a simple matrix combination in practical application.

The evaluation of regional comprehensive risk needs to introduce the n * 2 matrix of COVID-19 mass concentration D_i and the corresponding area percentage Pc_i in the horizontal and vertical research planes respectively in Equations 20 and 21.

Eq. 20-21:

$$A_{n*2}=\begin{bmatrix} D_{h_1} & Pc_{h_1} \\ D_{h_2} & Pc_{h_2} \\ \vdots & \vdots \\ D_{h_i} & Pc_{h_i} \\ \vdots & \vdots \\ D_{h_n} & Pc_{h_n} \end{bmatrix}, \quad \text{and } B_{n*2}=\begin{bmatrix} D_{h_1} & Pc_{h_1} \\ D_{h_2} & Pc_{h_2} \\ \vdots & \vdots \\ D_{h_i} & Pc_{h_i} \\ \vdots & \vdots \\ D_{h_n} & Pc_{h_n} \end{bmatrix}$$

Perform the difference product operation for the above A/B matrix and its inverse matrix to get Equations 22 and 23.

Eq. 22-23:

$$A_{n*2} \times B^{T}_{2*n}=C_{n*n}, \text{ and } A^{T}_{2*n} \times B_{n*2}=D_{2*2}$$

The values of Dh_i, Pch_i, Dv_i and Pcv_i are iterated 2^n times and n^2 times in C_{n*n} and C_{2*2} respectively According to the matrix value calculation method. However, the matrix C_{n*n} has higher calculation accuracy than the matrix D_{2*2} when n>2. Therefore, this study chooses the iterative calculation expression of the matrix C_{n*n} on different research surfaces taking the calculation significance of mass concentration and contaminated area percentage into account, and interchanges the $B^T{}_{2*n}$ rows, and the expansion calculation is as follows.

$$\begin{bmatrix} D_{h_1}*Pc_{h_1}+D_{v_1}*Pc_{v_1} & \cdots & D_{h_1}*Pc_{h_{(i-1)}}+D_{v_1}*Pc_{v_1} & D_{h_1}*Pc_{v_i}+D_{v_i}*Pc_{h_1} & \cdots & D_{h_1}*Pc_{v_n}+D_{v_n}*Pc_{h_1} \\ \vdots & \ddots & \vdots & \vdots & \ddots & \vdots \\ D_{h_{(i-1)}}*Pc_v+D_{v_1}*Pc_{h_{(i-1)}} & \cdots & D_{h_{(i-1)}}*Pc_{v_{(i-1)}}+D_{v_{(i-1)}}*Pc_{h_{(i-1)}} & D_{h_{(i-1)}}*Pc_{v_i}+D_{v_i}*Pc_{h_{(i-1)}} & \cdots & D_{h_{(i-1)}}*Pc_{v_n}+D_{v_n}*Pc_{h_{(i-1)}} \\ D_{h_i}*Pc_{v_i}+D_{v_i}*Pc_{h_i} & \cdots & D_{h_i}*Pc_{v_{(i-1)}}+D_{v_{(i-1)}}*Pc_{h_i} & D_{h_i}*Pc_{v_i}+D_{v_i}*Pc_{h_i} & \cdots & D_{h_i}*Pc_{v_n}+D_{v_n}*Pc_{h_i} \\ \vdots & \ddots & \vdots & \vdots & \ddots & \vdots \\ D_{h_n}*Pc_{v_1}+D_{v_1}*Pc_{h_n} & \cdots & D_{h_n}*Pc_{v_{(i-1)}}+D_{v_{(i-1)}}*Pc_{h_n} & D_{h_n}*Pc_{v_i}+D_{v_i}*Pc_{h_n} & \cdots & D_{h_n}*Pc_{v_n}+D_{v_n}*Pc_{h_n} \end{bmatrix}$$

In this study, the difference product of the horizontal A_{n*2} Matrix and the B_{2*n} Matrix is used to obtain the n * n square Matrix. The Comprehensive Pollution Disturbance (CPD) of the horizontal and vertical coupling C_{n*n} Matrix can be expressed as follows when n=100:

$$CPD=1.70692*10^{-19}kg/m^3$$

The CPD represents the comprehensive pollution index of the horizontal and vertical personnel activity plane under the current building scheme and meteorological conditions. It can be used to: (1) compare the building and planning scheme at the design stage; (2) evaluate the risk of different positions in different directions in the completed residential area, and (3) new window ventilation design in the city reconstruction aiming at the minimum of CPD to generate social and economic value.

6 Conclusions

Through the numerical study of the design scheme of Gaozhu Innovation Base, this paper reaches conclusions on the optimization of the building scheme from the quantitative and qualitative analysis in combination with the current requirements of the urban healthy ventilation during the undergoing epidemic situation, providing new design methods for future urban design beyond traditional architectural design standards. Conclusions can be drawn from the theoretical research and case analysis as follows.

(1) The amplification coefficients of urban disturbance in the wind speed direction of the Innovation Base are respectively σ_1=0.047 representing safe evacuation distance for ventilation of new buildings downstream, and σ_2=0.403 representing origin airflow disturbance retreat of new buildings downstream in the horizontal direction. The amplification coefficients of urban disturbance in the height direction of the Innovation Base are respectively σ_3=1.26 representing the control range of the skyline of new buildings, and σ_4=4.38 representing the urban canopy ventilation boundary in practical.

(2) The Comprehensive Risk Coefficient (CRC) of the Innovation Base in the horizontal direction is CRC_h=17.88, and the Comprehensive Risk Coefficient in the vertical direction is CRC_v=102.97. The risk of infection of personnel on the vertical contact surface is 5.76 times greater than that on the horizontal contact surface in the building cluster, so more outdoor activities are suggested rather than arbitrary window ventilation once the public safety event of COVID-19 breaks out in the Innovation Base.

(3) The Comprehensive Pollution Disturbance (CPD) of the horizontal and vertical coupling Matrix C_{n*n} of the Innovation Base is $1.70692*10^{-19}kg/m^3$ representing the safety index of the Innovation Base in large public health safety events.

In conclusion, this study contributes to effective support of architectural design and urban design facing safe ventilation in the new era, providing theoretical support for the risk assessments as well as the resident control and anti-epidemic policies for both governments and urban residents during

the repeating worldwide epidemic situation.

7 Outlook

Although this study has carried out a series of theoretical studies, field tests and formula derivation for urban safe ventilation design based on epidemic spread, there is still further improvement which is required in the future.

(1) Although CFD technology has developed for decades from the last century, each calculation model still has its limitations in practical application with their development today, there is still necessity for appropriate models aimed at different research objectives in the future.

(2) Due to the complexity of building facades, greening design, topography and meteorological conditions, the simulation research cannot fully reflect the urban ventilation environment in reality.

(3) The occurrence of every epidemic situation is accompanied by their inherent toxicological principles and epidemiology principles with constantly evolving. The urban safety ventilation still needs to be combined with the biological characteristics of the pollution source in epidemic prevention strategies in the future.

With the continuous improvement of the urbanization and people's continuous pursuit of a healthy life worldwide, urban ventilation will still be an important research topic in the field of Human Sustainable Development.

Acknowledgement

Thanks to the platform support and financial support of "Chongqing Municipal Construction Technology Plan (No. 20220184)", "Chongqing Municipal Postdoctoral Research Flow Project Special Grant (No. 2211013357670761)" and "Natural Science Foundation of Chongqing Municipal (No. CSTB2022NSCQ-MSX1430)". The authors declare that there is no conflict of interest in the content of this study.

References

1. Xu, G., et al., *How does urban population density decline over time? An exponential model for Chinese cities with international comparisons.* Landscape and Urban Planning, 2019. **183**: p. 59-67.
2. Yang, L., et al., *Emergency response to the explosive growth of health care wastes during COVID-19 pandemic in Wuhan, China.* Resources, Conservation and Recycling, 2021. **164**: p. 105074.
3. Cruz, M.P., et al., *COVID-19, a worldwide public health emergency.* Revista Clínica Española (English Edition), 2021. **221**(1): p. 55-61.
4. Nair, R., et al., *Predicting the Death Rate Around the World Due to COVID-19 Using Regression Analysis.* International Journal of Swarm Intelligence Research (IJSIR), 2022. **13**(2): p. 1-13.
5. Zheng, Y., et al., *Bioaerosols of yesterday, today and tomorrow.* Chinese Science Bulletin, 2018. **63**(10), in Chinese.
6. Li, X.X, et al., *Types of pathogenic microorganisms in indoor air and an overview of detection techniques*. Science bulletin, 2018. **63**(21): p. 12, in Chinese.
7. Liu, W., *Study on indoor and outdoor diffusion and risk of microbial aerosols in natural wind velocity field*. 2010, Doctoral Thesis, Tianjing University, in Chinese.
8. Peng, Y.L., et al., *Indices employed for the assessment of "urban outdoor ventilation" - A review.* Atmospheric Environment, 2020. **223**.
9. Lu, X., Y. Lei, and C. Chen, *Study on the Wind Environment and Pollution Diffusion of Building Group Based on LES Staggered Joint Arrangement.* Journal of Aerospace Engineering, 2022. **35**(1): p. 04021116.
10. Mahjoub, H., et al., *Near Source Modeling of Pollutant Emissions From an Elevated Source Over an Urban Area Under Cross High Ventilation.* Journal of Thermal Science and Engineering Applications, 2022. **14**(3).
11. Palusci, O., et al., *Impact of morphological parameters on urban ventilation in compact cities: The case of the Tuscolano-Don Bosco district in Rome.* Science of the Total Environment, 2022. **807**.
12. Hang, J., et al., *On the influence of viaduct and ground heating on pollutant dispersion in 2D street canyons and toward single-sided ventilated buildings.* Atmospheric Pollution Research, 2016. **7**(5): p. 817-832.
13. Hofman, J., et al., *Influence of tree crown characteristics on the local PM10 distribution inside an urban street canyon in Antwerp (Belgium): A model and experimental approach.* Urban Forestry & Urban Greening, 2016. **20**: p. 265-276.
14. Su, N., et al., *Experimental and numerical evaluation of wind-driven natural ventilation and dust suppression effects of coal sheds with porous gables.* Building and Environment, 2020. **177**.
15. Pullen, J., et al., *A comparison of contaminant plume statistics from a Gaussian puff and urban CFD model for two large cities.* Atmospheric Environment, 2005. **39**(6): p. 1049-1068.
16. Nakayama, H., T. Takemi, and T. Yoshida, *Large-Eddy Simulation of Plume Dispersion in the Central District of Oklahoma City by Coupling with a Mesoscale Meteorological Simulation Model and Observation.* Atmosphere, 2021. **12**(7): p. 889.
17. Dai, Y.W., et al., *Investigation of interunit dispersion in 2D street canyons: A scaled outdoor experiment.* Building and Environment, 2020. **171**.
18. Yuan, C., et al., *A modelling-mapping approach for fine-scale assessment of pedestrian-level wind in high-density cities.* Building and Environment, 2016. **97**: p. 152-165.
19. Mei, S.J., et al., *Street canyon ventilation and airborne pollutant dispersion: 2-D versus 3-D CFD simulations.* Sustainable Cities and Society, 2019. **50**.
20. Bauer, T.J., *The Effect of the Urban Parametrization on Simulated Contaminant Atmospheric Transport and Dispersion.* Boundary-Layer Meteorology, 2019. **170**(1): p. 95-125.
21. Yang, F., et al., *Simulations of the impacts of building height layout on air quality in natural-ventilated rooms around street canyons.* Environmental Science and Pollution Research, 2017. **24**(30): p. 23620-23635.
22. Wang, J.H., et al., *Assessment of Pollutant Dispersion in the Re-entrance Space of a High-rise Residential Building, Using Wind Tunnel Simulations.* Indoor and Built Environment, 2010. **19**(6): p. 638-647.
23. Yuan, C., et al., *Multilayer urban canopy modelling and mapping for traffic pollutant dispersion at high density urban areas.* Science of the Total Environment, 2019. **647**: p. 255-267.
24. Jana, A., A. Sarkar, and R. Bardhan, *Analysing outdoor airflow and pollution as a parameter to assess the compatibility of mass-scale low-cost residential development.* Land Use Policy, 2020. **99**: p. 105052.
25. Liu, Y.S., et al., *Study on micro-atmospheric environment by coupling large eddy simulation with mesoscale model.* Journal of Wind Engineering and Industrial Aerodynamics, 2012. **107**: p. 106-117.
26. Hang, J., et al., *City breathability in medium density urban-like geometries evaluated through the pollutant transport rate and the net escape velocity.* Building and Environment, 2015. **94**: p. 166-182.
27. Gromke, C., N. Jamarkattel, and B. Ruck, *Influence of roadside hedgerows on air quality in urban street canyons.* Atmospheric Environment, 2016. **139**: p. 75-86.

28. Ramponi, R., et al., *CFD simulation of outdoor ventilation of generic urban configurations with different urban densities and equal and unequal street widths.* Building and Environment, 2015. **92**: p. 152-166.
29. Li, X.-X., R. Britter, and L.K. Norford, *Effect of stable stratification on dispersion within urban street canyons: A large-eddy simulation*. Atmospheric environment, 2016. **144**: p. 47-59.
30. Habilomatis, G. and A. Chaloulakou, *A CFD modeling study in an urban street canyon for ultrafine particles and population exposure: The intake fraction approach.* Science of the Total Environment, 2015. **530**: p. 227-232.
31. Oaks, W.R., K. Flora, and A. Khosronejad, *Eulerian numerical modeling of contaminant transport in Lower Manhattan, New York City, from a point-source release under the dominant wind condition: Insights gained via LES.* 2021.
32. Chang, C.-H., et al., *Numerical simulations and wind tunnel studies of pollutant dispersion in the urban street canyons with different height arrangements.* Journal of Marine Science and technology, 2013. **21**(2): p. 2.
33. Song, J., et al., *Natural ventilation in cities: the implications of fluid mechanics.* Building Research & Information, 2018. **46**(8): p. 809-828.
34. Chen, L., et al., *The influence of building packing densities on flow adjustment and city breathability in urban-like geometries.* Procedia engineering, 2017. **198**: p. 758-769.
35. Adamek, K., et al., *Pedestrian level wind assessment through city development: A study of the financial district in Toronto.* Sustainable cities and society, 2017. **35**: p. 178-190.
36. Lin, Y., et al., *Investigation of the Reynolds number independence of cavity flow in 2D street canyons by wind tunnel experiments and numerical simulations.* Building and Environment, 2021. **201**: p. 107965.
37. Chew, L.W., L.R. Glicksman, and L.K. Norford, *Buoyant flows in street canyons: Comparison of RANS and LES at reduced and full scales.* Building and Environment, 2018. **146**: p. 77-87.
38. Huang, J.X., et al., *Outdoor Airborne Transmission of Coronavirus Among Apartments in High-Density Cities.* Frontiers in Built Environment, 2021. **7**.
39. C, Y.L.A.B., et al., *A multidimensional model for green building assessment: A case study of a highest-rated project in Chongqing.* Energy and Buildings, 2016. **125**: p. 231-243.
40. A, B.J.H., L.D. A, and D.P. B, *Wind-sensitive urban planning and design: Precinct ventilation performance and its potential for local warming mitigation in an open midrise gridiron precinct.* Journal of Building Engineering. **29**.
41. Bao-Jie, et al., *Enhancing urban ventilation performance through the development of precinct ventilation zones: A case study based on the Greater Sydney, Australia - ScienceDirect.* Sustainable Cities and Society. **47**(C): p. 101472-101472.
42. Li, Y.Q., et al., *A method to identify individually physiological response differences to heat exposure using Comprehensive Deviation Coefficient (CDC).* Energy and Buildings, 2020. **217**.